



Interactions of small gold clusters, Au_n (n = 1–3), with graphyne: Theoretical investigation



Elmira Azizi, Zahra Aliakbar Tehrani, Zahra Jamshidi*

Chemistry and Chemical Engineering Research Center of Iran, P.O. Box 14335-186, Tehran, Iran

ARTICLE INFO

Article history:

Accepted 22 September 2014

Available online 2 October 2014

Keywords:

Graphyne

Gold cluster

Surface sensors

Energy decomposition analysis

Charge transfer

ABSTRACT

The interactions of gold atom and clusters (Au₂ and Au₃) with the active sites of graphyne (GY) have been investigated using density functional theory (PBE, PBE-D3, and B3LYP-D3). In order to compare performance of DFT functional (BP86, PBE, TPSSH, B3LYP, PBE-D3, TPSSH-D3, and B3LYP-D3), the interactions of Au₂ with various functional groups such as —sp, —sp² and aromatic sp² carbon atoms, —sp, —sp² and aromatic sp²-bonds have been investigated and also compared with the ab initio MP2 results. Additionally, the nature of interactions for graphyne–Au₂ complexes are interpreted by means of the natural bond orbital (NBO), the quantum theory of atoms in molecules (QTAIM) and energy decomposition analysis (EDA) and compared with those of related graphene–Au₂. This study suggests that graphyne shows complex behavior in comparison to those of graphene and could also be useful in modeling of the next generation electronic devices.

© 2014 Elsevier Inc. All rights reserved.

1. Introduction

One-atom thick carbon sheet structure has been regarded as one of the most promising future electronic materials due to its unique mechanical and electronic properties resulted from the two-dimensional 2D atomic structure [1–3]. As a new form of non-natural carbon allotrope related to graphite/graphene (GR), graphyne (GY) has been the subjects of interest due to their unique structures and intriguing electronic, optical and mechanical properties [4,5] and also promising nanoelectronics and energy storage applications [6]. Graphyne was first proposed in 1987 by Baughman et al. [7] but despite of many attempts [8–12] the synthesis of graphyne has not yet been reported. Graphite consist of a variation of the —sp² carbon motif forming graphene, which can be thought of as simply replacing a portion of the characteristic graphitic carbon bonds by acetylene (single- and triple-bond) carbon-like chains [13,14]. The presence of the —sp carbon atoms in a hexagonal lattice of the graphyne leads to various types of configurations and properties [5,15–22].

Lacking experimental data, knowledge of the properties of this promising and interesting carbon allotrope depends on theoretical predictions. Graphynes [4,7], are favorable candidates for the engineering of novel graphene-like materials which have

promising electronic, optical, and mechanical properties [7,23–27]. Kang et al. [5] examined elastic, electronic and optical properties of the c-graphyne with first-principle calculations in which one-third of the carbon–carbon graphene bonds being replaced by the acetylenic linkages. The energy storage capacities of γ-graphyne or graphdiyne were investigated with ab initio first-principle calculations [5,6,20]. Through other studies, graphyne revealed extraordinary potential in energy storage applications especially in the storage of hydrogen and lithium. Malko et al. [19] discovered that α-, β- and 6,6,12-graphynes have electronic structure similar to graphene and the latter (6,6,12-graphyne) shows more amazing electronic properties than that of graphene.

Absorbance of metals on single layer carbon, i.e. graphene, was employed for various parts of electrical devices, such as electrical connections [28], gate dielectrics [29], tunnel barriers [30], and also active catalysts, and energy storage devices [31,32]. Previous work shown that a single adsorbed 3d transition metal atom (V, Cr, Mn, Fe, Co and Ni) on GY (TM-GY) promotes the magnetization of the system, which suggests its potential in spintronics [33–35]. Sun and co-workers investigated the electronic and magnetic properties of one-dimensional zigzag and armchair 3d transition metal nanowires on graphyne (GY), using density functional theory plus Hubbard U (DFT1U) [35]. Among these metallic adsorbents, gold has been considered as one of the most interesting and fantastic candidates [36]. The effect of Au nanoparticles on the electronic structure of graphene has been studied theoretically [37]. A recent work has emphasized the effects of distribution of

* Corresponding author. Tel.: +98 2144580711.

E-mail addresses: jamshidi@ccerci.ac.ir, na.jamshidi@gmail.com (Z. Jamshidi).

Au atoms on the charge carrier mobility of graphene [38]. They have concluded that the formation of Au clusters increases the mobility whereas a homogeneous distribution reduces it. Amft et al. [39] studied theoretically the effect of variation of size of small Au clusters adsorbed on graphite by focusing on an analysis of the electronic structures which confirmed previous results.

Recent studies indicate that graphyne is potentially superior to graphene in directional electrical conductivity [19]. However, to our knowledge the effect of adsorption of gold nano-structure on the surface of graphyne has not been reported yet. Studying interactions between small gold clusters and graphyne and their effects on the electronic properties of graphyne is highly beneficial for the accomplishment of future nanoscale devices and fulfillment of their promising applications. Therefore, the objective of this research was to establish the influence of gold clusters adsorption on electronic properties of graphyne surface. To aim this purpose the nature of graphyne–Au_{1–3} interactions have been investigated by quantum chemical methods, which are widely used for analyzing the chemical bonds in transition metal containing compounds: Natural Bond Orbital analysis (NBO), quantum theory of atoms-in-molecules (QTAIM) and energy decomposition analysis (EDA). Furthermore, we try to answer the question “how different hybridization nature of carbon atoms in graphyne (GY) can affect its complexation behavior with gold cluster compared to graphene (GR)” by obtained results of above mentioned analysis.

2. Computational details

The interactions of Au₂ with the *sp*, *sp*² and aromatic *sp*² carbon atom, *sp*, *sp*², and aromatic-*sp*² bonds and also hollow site of aromatic motif have been investigated by MP2 method and different DFT functionals, including recent dispersion corrected Grimme's density functionals (PBE-D3, TPSSH-D3, and B3LYP-D3) [40] and some common and well-established other ones (BP86, PBE, TPSSH, and B3LYP) [41–44]. The geometries of graphyne complexes with gold metal clusters were fully optimized by PBE and PBE-D3 functionals. The exchange correlation energy functional was used with the general gradient approximation (GGA) in the Perdew–Burke–Ernzerhof scheme. In addition, binding energies for the optimized PBE-D3 geometries have been obtained as well by B3LYP-D3 functional. The Def2-TZVP [45] basis set was applied to Au, C, and H atoms, in these basis sets, 19 outermost electrons of gold are explicitly described by the (11s 5p 5d 3f 3g)/[8s 5p 5d 2f 3g] basis. The harmonic vibrational frequencies were calculated for all the optimized geometries, and real frequencies were detected in all cases. The binding energy E_b of the complex, GY–Au_{1–3}, is defined in a standard way as the absolute value of the energy difference $E_b = E_{\text{GY–Au}_{1-3}} - (E_{\text{GY}} + E_{\text{Au}_{1-3}})$ and its ZPVE-corrected values are reported throughout this work. These calculations have been done using ORCA 2.9 suite of programs [46].

To reveal the nature of mentioned interactions, the NBO, QTAIM, and EDA analyses were carried out on the PBE-D3 optimized structures. The NBO analysis was performed on these structures to calculate charge transfer and Natural population analysis (NPA) [47,48]. The electron density, $\rho(r)$ and its Laplacian, $\nabla^2\rho(r)$, at the bond critical points (BCPs) were computed based on Bader's QTAIM [49], using AIM2000 [50] program. The EDA was done using the program package ADF (2010, 01) [51–53], which is based on the work by Ziegler and Rauk [54], and Morokuma [55]. The bonding analysis was carried out at the BP86-D3/TZ2P level of theory, while scalar relativistic effects have been considered using the zero-order regular approximation (ZORA) [56–58].

3. Results and discussion

Our first intent was to identify a computational method that is less computationally demanding than MP2. We then planned to use this method to study the binding of gold atom and clusters (Au₂ and Au₃) with graphyne surface. Therefore, we initially studied smaller systems as models of the graphyne surface: the *sp* and *sp*² carbon atoms (from C₂H₂ and C₂H₄ molecules, respectively) and three different positions of benzene carbon atoms ('top' site directly above a C atom, a 'bridge' site above the midpoint of a C–C bond, and the 'hollow' site above the center of the aromatic ring). The equilibrium bond lengths and binding energies for interactions of Au₂ cluster with these models have been investigated based on MP2 and different DFT functionals (such as PBE-D3, TPSSH-D3, B3LYP-D3, BP86, PBE, TPSSH, and B3LYP) are given in Table 1. All of the potential energy curves for these complexes are given in Figs. S1–S3 in Supplementary Materials.

Comparison of the binding energies of Au₂ cluster with the *sp* and *sp*² C–C bonds and the aromatic *sp*²-bonds (Au₂...*sp*-b, Au₂...*sp*²-b and Au₂...aromatic *sp*²-b complexes in Table 1 in which Au₂ cluster oriented above the midpoint of C–C bond) displays that the Au₂...*sp*²-b complex is more stable than the Au₂...*sp*-b and Au₂...aromatic *sp*²-b complexes. Based on MP2 results, the binding energy of Au₂...*sp*²-b complex ($E_b = -25.5$ kcal/mol) is about 11% and 24% higher than those of Au₂...*sp*-b ($E_b = -22.6$ kcal/mol) and Au₂...aromatic *sp*²-b ($E_b = -19.4$ kcal/mol) complexes, respectively. For interactions of Au₂ cluster with top site of *sp* and *sp*² carbon atoms (Au₂...*sp*-a and Au₂...*sp*²-a complexes in Table 1), values of E_b are almost less stable than complexes in which Au₂ cluster oriented above the midpoint of C–C bonds.

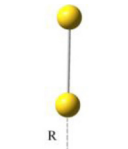
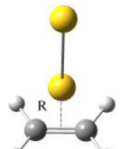
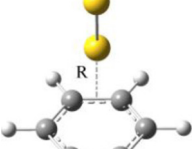
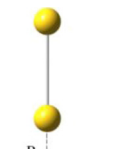
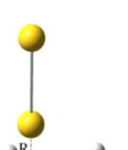
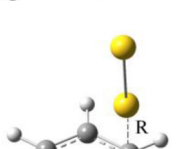
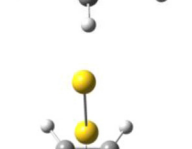
However, all of these complexes are more stable than complex in which the gold cluster occupied the 'hollow' site above the center of the aromatic ring (Au₂...aromatic *sp*²-c complex in Table 1). It should be mentioned that, the same relative order of binding energy obtained by other functionals. The PBE-D3 and TPSSH-D3 methods overestimate the binding energy (less than 30%) in comparison with MP2 values. In the case of the bond lengths, the difference between these methods in prediction of bond lengths is about 0.1 Å. For most of the investigated complexes, binding energies obtained at B3LYP-D3 level have least difference with the MP2 results, but the B3LYP-D3 method overestimates the bond length values in comparison with other DFT and MP2 values. Therefore, based on these results, B3LYP-D3 binding energies of the optimized structure of PBE-D3 were used to investigate the interactions of gold atom and its clusters (Au₂ and Au₃) with the active sites of graphyne.

3.1. Energetic and structures

The optimized structure of graphyne surface considered in this study characterize as follow: the triple bond length is 1.22 Å and the single bond is 1.42 Å (slightly shorter than the typical value of 1.47 Å). The aromatic bond length is 1.41 Å, slightly shorter than that of a pristine graphene sheet (1.43 Å) due to the presence of the acetylene groups. All possible initial sites (positions 1–5) for adsorption of gold atom and its clusters (Au₂ and Au₃) on the graphyne surface are shown in Fig. 1. Unlike graphene, there are several attachment sites for gold atoms on the graphyne, i.e., on top of the *sp* and *sp*² carbon atoms, in the hollow sites of *sp* and *sp*²-bonded hexagons and *sp*-bonded triangles.

Studying the electrostatic potentials is a means of understanding the electronic contribution to the leaning effect and whether they are related to the geometric features which are observed from structural studies. The electrostatic potential surface of the graphyne was generated by mapping 6-31G** electrostatic potentials onto surfaces of molecular electron density (0.02 electron/Å) and

Table 1
Comparison the binding energies (in kcal/mol) and bond lengths (in Å) for $C_2H_2-Au_2$, $C_2H_4-Au_2$, and $C_6H_6-Au_2$ complexes.

Complex		BP86	PBE	TPSSH	B3LYP	PBE-D3	TPSSH-D3	B3LYP-D3	MP2
$Au_2 \dots sp-b$		E_b	−23.0	−24.3	−22.1	−17.1	−24.8	−18.7	−22.6
		R	2.08	2.08	2.08	2.16	2.08	2.08	2.00
$Au_2 \dots sp^2-b$		E_b	−27.4	−29.0	−26.5	−20.4	−29.2	−19.3	−25.5
		R	2.16	2.16	2.16	2.26	2.16	2.26	2.16
$Au_2 \dots aromatic\ sp^2-b$		E_b	−20.6	−22.4	−20.4	−15.0	−24.0	−19.6	−19.4
		R	2.26	2.26	2.26	2.36	2.26	2.36	2.17
$Au_2 \dots sp-a$		E_b	−20.0	−21.4	−18.7	−14.4	−21.9	−15.7	−15.3
		R	2.12	2.12	2.12	2.26	2.12	2.26	2.22
$Au_2 \dots sp^2-a$		E_b	−22.5	−23.9	−21.48	−16.80	−23.99	−16.81	−16.10
		R	2.18	2.18	2.18	2.29	2.18	2.29	2.18
$Au_2 \dots aromatic\ sp^2-a$		E_b	−20.5	−22.2	−20.1	−15.1	−23.8	−19.7	−18.0
		R	2.26	2.26	2.26	2.26	2.26	2.36	2.16
$Au_2 \dots aromatic\ sp^2-c$		E_b	−11.8	−13.6	−12.8	−9.2	−15.2	−13.9	−10.2
		R	2.39	2.39	2.36	2.59	2.39	2.70	2.15

color-coding, using the program Spartan [59]. In this surface which has shown in Fig. 1 for graphyne (and also Fig. 3 for graphyne- Au_{1-3} complexes) the potential energy values range from +100 kJ/mol to −100 kJ/mol (with blue as the highest and red as the lowest electrostatic potential energy values). As shown in Fig. 1, several high

electron density domains can be observed in graphyne: one around each atomic nucleus, one enclosing the internuclear region corresponding to the $-C=C-$ aromatic double bond, and one enclosing the internuclear region corresponding to the $-C\equiv C-$ triple bond. The region represented by red color, appearing below and above

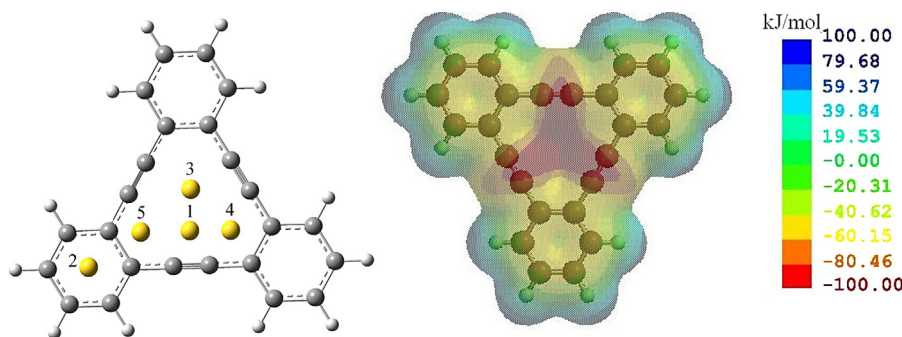


Fig. 1. Schematic illustration of Au_{1-3} adsorption active sites on graphyne.

the hollow sites of $-\text{sp}$ and $-\text{sp}^2$ -bonded hexagons of graphyne, is the most electron rich region in this molecule and could be the center for electrophilic activity. These sites can donate electron density via their lone pairs to the 5d and 6s orbitals of gold atoms. We think that in the real two dimensional graphyne this position also remains as the most electron rich region and therefore, plays the main role to transition metal absorption. This model can be suitable for prediction of the binding site of gold atom and clusters (Au_2 and Au_3) on the real two dimensional graphyne.

The optimized structural parameters for the most stable complexes of graphyne with gold atom, Au_2 and Au_3 clusters (Au_{1-3}) obtained at the PBE-D3 level are shown in Fig. 2. As would be seen in Fig. 2, gold atom located on top of the $-\text{sp}$ and $-\text{sp}^2$ carbon atoms of GY with Au–C bond lengths of 1.98 (in GY–Au-a complex) and 2.08 Å (in GY–Au-b complex) with binding energies of –25.1 and –16.7 kcal/mol, respectively. However, for the most stable Au–GY complex gold atom located in-plane and slightly off the center of a hexagon, i.e., GY–Au-c complex in Fig. 2, where the distance between the Au atom and the nearest C atom of GY is 2.14 Å with the binding energy value of –25.4 kcal/mol. For these GY–Au complexes, Au atom donating charge to GY and the amount of charge transferred from Au to GY is mainly larger in the GY–Au-c complex than the others.

For GY– Au_2 complexes, gold dimer was absorbed on GY vertically through one gold atom or parallel to the carbon sheet by two Au atoms (GY– Au_2 -a, GY– Au_2 -b and GY– Au_2 -c complexes in Fig. 2). In the former case, Au_2 interacts with the $-\text{sp}$, $-\text{sp}^2$ bonded carbon, and middle of triangular hollow site with Au–C bond lengths of 2.12 (GY– Au_2 -a), 2.18 (GY– Au_2 -b), and 2.00 Å (GY– Au_2 -c) and binding energy values of –32.7, –25.0, and –20.9 kcal/mol, respectively. Furthermore, Au–Au cluster prefers to be attached on a consisting $-\text{sp}$ bonded carbon atoms parallel to the $-\text{C}\equiv\text{C}-$ bond or top of the triangular hollow site, and in both cases the Au atom interact with $-\text{sp}$ carbon atom. As you can find in Fig. S4 in Supplementary Materials, for this orientation, the interaction of gold atom with $-\text{sp}$ carbon atom is stronger than Au–Au dissociation energy (GY– Au_2 -d). However, in GY– Au_2 -e complex, each Au atom interacted at the same time with $-\text{sp}$ carbon atoms, which causes the dissociation of aromatic $-\text{C}\equiv\text{C}-$ bonds.

The Au_3 cluster was adsorbed on the GY sheet in which one gold atom of Au_3 cluster oriented to $-\text{C}\equiv\text{C}-$ bond (GY– Au_3 -a complex in Fig. 2), and the interactions with $-\text{sp}$ carbons via two gold atoms of Au_3 cluster (GY– Au_3 -b complex in Fig. 2). In these complexes, the Au–C bond lengths are slightly the same as the one observed in Au_2 –GY complexes. However, the binding energies for the adsorption of Au_3 cluster on GY sheet are –44.8 and –44.2 kcal/mol for GY– Au_3 -a and GY– Au_3 -b, respectively.

As mentioned in the introduction, GY consists of a diversity of the $-\text{sp}^2$ carbon motif forming graphene by replacing a portion of the characteristic graphitic carbon bonds with acetylene. Therefore, it can be anticipated that the binding of gold clusters with the

Table 2

Binding energies (in kcal/mol) and NPA Charge difference for GY– Au_{1-3} complexes.

Complex	E_b^{PBE}	$E_b^{\text{PBE-D3}}$	$E_b^{\text{B3LYP-D3}}$	Δq^a
GY–Au-a	–25.27	–25.13	–11.43	0.143
GY–Au-b	–16.64	–16.65	–4.68	0.074
GY–Au-c	–25.40	–25.40	–	0.885
GY– Au_2 -a	–33.11	–32.68	–17.80	0.025
GY– Au_2 -b	–26.32	–24.99	–13.10	0.045
GY– Au_2 -c	–20.89	–20.89	–12.31	–0.091
GY– Au_3 -a	–34.45	–44.82	–25.46	0.113
GY– Au_3 -b	–18.20	–44.23	–26.58	0.418
GR– Au_2 -b	–23.38	–23.27	–13.37	0.022
GR– Au_2 -h	–23.96	–23.86	–5.50	–0.022
GR– Au_2 -t	–23.98	–23.87	–14.80	0.004

^a $\Delta q = q_{\text{Au}_{1-3}}(\text{complexed}) - q_{\text{Au}_{1-3}}(\text{isolated})$.

graphyne are more stable than the corresponding binding with the graphene. Such phenomena originate from the different hybridization nature of carbon atoms in graphene (GR) and graphyne (GY). There are only $-\text{sp}^2$ carbon atoms in graphene; however, the $-\text{sp}$ carbon atoms in graphyne play a key role in the absorption process. On the other hands, the in-plane π/π^* orbital in GY can rotate toward any direction perpendicular to the line of $-\text{C}\equiv\text{C}-$, therefore the valence electrons of the gold clusters can easily couple with these π/π^* orbitals, which produces the gold clusters to adsorb in GY surface with more favorable energy. In the next section, the nature of Au_2 cluster interactions with GY and GR has been compared in details. The optimized structures and binding energy values for complexes of graphene with Au_2 cluster (GR– Au_2 -b, GR– Au_2 -h and GR– Au_2 -t complexes) are given in Fig. 2 and Table 2.

3.2. Analysis of the nature of interactions

The nature of graphyne and graphene interactions with Au_2 cluster have been discussed by natural bond orbital (NBO), quantum theory of atoms-in-molecules (QTAIM), and energy decomposition analysis (EDA) methods, which are widely used for analyzing the chemical bonds in transition metal containing compounds:

(a) *Natural Bond Orbital analysis.* A second-order perturbation theory analysis of the Fock matrix was carried out to evaluate the donor–acceptor interaction on the NBO basis. The charge transfer energy values (ΔE_{CT}) between donor–acceptor orbitals in GY– Au_2 and GR– Au_2 complexes are given in Table 3. In these complexes, charge is transferred from the lone pair orbital of Au_2 cluster to anti-bonding σ^* and π^* orbitals of C–C bond, and also back donation from bonding σ and π orbitals of C–C bond to the anti-bonding σ^* and n^* orbitals of Au_2 cluster. Values of transferred charge in donation and back donation processes, Δq_{CT} , have been calculated and given in Table 3. Comparative values of ΔE_{CT} with E_b for these complexes revealed that charge transfer energies have the same trend as binding energies. As expected, for the GY– Au_2 complexes,

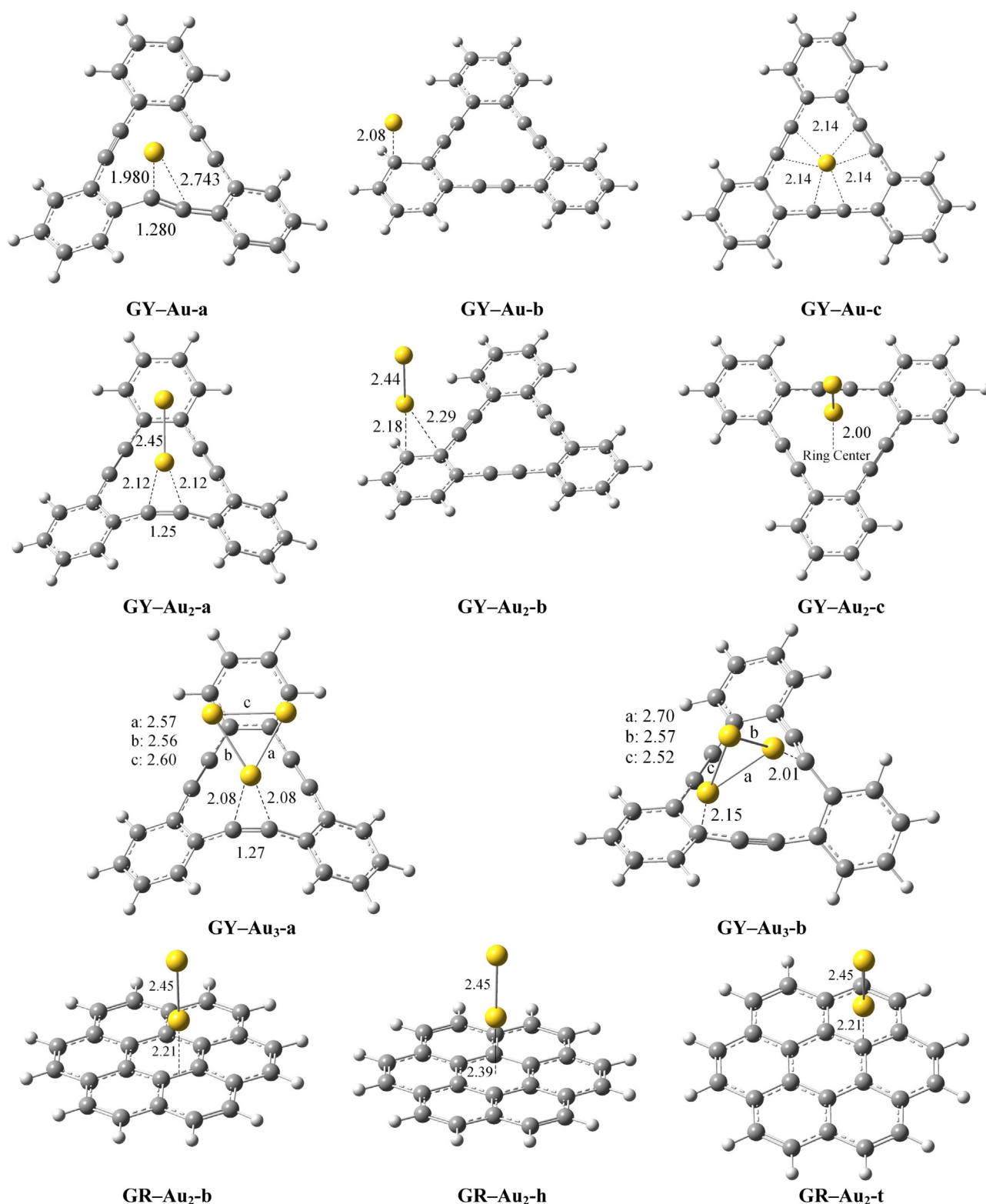


Fig. 2. Optimized geometries of GY-Au₁₋₃ and GR-Au₂ complexes obtained at PBE-D3 level. Distances are reported in Å.

ΔE_{CT} and Δq_{CT} are significantly more than those of the GR-Au₂ complexes. Therefore, charge transfer played the critical role in the interaction between GY and gold cluster.

Moreover, natural population analysis (NPA) has been performed on optimized structures. In all of the investigated complexes the interacting Au atom carries a positive charge after complexation. It is evident that in most of these complexes the

charge differences in Au₂ cluster, ($\Delta q_{Au_2} = q_{Au_2}(\text{complexed}) - q_{Au_2}(\text{isolated})$) are positive, and dominant part of the charge is transferred from gold cluster to the graphyne and graphene. Just for GY-Au₂-c and GR-Au₂-h complexes (in which Au₂ cluster interacted through the middle of ring with GY and GR) the Δq_{Au_2} is negative, and charge is only transferred from σ and π orbitals of C–C bond to n^* and σ^* orbitals of Au₂ cluster. Comparison of the

Table 3

Calculated NPA charges and charge transfer feature based on NBO theory.

Complex	Charge transfer	ΔE_{CT}	q_{Au}	$\Delta q_{Au_2}^a$	Δq_{CT}	E_b
GY–Au ₂ -a	$\sigma_{C33-C34} \dots n^*_{Au}$	6.21	0.246	0.025	0.007	–32.68
	$\pi_{C33-C34} \dots n^*_{Au}$	26.83			0.043	
	$\pi_{C33-C34} \dots \sigma^*_{Au-Au}$	25.23			0.058	
	$n_{Au} \dots \pi^*_{C33-C34}$	32.22			0.171	
GY–Au ₂ -b	$\sigma_{C2-C3} \dots n^*_{Au}$	4.65	0.222	0.045	0.005	–24.99
	$\pi_{C2-C3} \dots n^*_{Au}$	18.45			0.027	
	$\pi_{C2-C3} \dots \sigma^*_{Au-Au}$	17.75			0.050	
	$n_{Au} \dots \pi^*_{C2-C3}$	25.46			0.193	
GY–Au ₂ -c	$\sigma_{C31-C32} \dots n^*_{Au}$	1.71	0.061	–0.091	0.003	–20.89
	$\pi_{C31-C32} \dots \sigma^*_{Au-Au}$	1.79			0.004	
	$\pi_{C31-C32} \dots n^*_{Au}$	1.53			0.002	
	$\sigma_{C33-C34} \dots n^*_{Au}$	1.40			0.002	
	$\pi_{C33-C34} \dots \sigma^*_{Au-Au}$	1.79			0.004	
	$\pi_{C33-C34} \dots n^*_{Au}$	1.55			0.002	
	$\sigma_{C35-C36} \dots \sigma^*_{Au}$	1.18			0.002	
	$\pi_{C35-C36} \dots \sigma^*_{Au-Au}$	1.79			0.004	
	$\pi_{C35-C36} \dots n^*_{Au}$	1.54			0.002	
GR–Au ₂ -b	$\sigma_{C1-C2} \dots n^*_{Au}$	3.25	0.173	0.022	0.003	–23.27
	$\sigma_{C1-C7} \dots n^*_{Au}$	3.24			0.003	
	$\pi_{C1-C7} \dots n^*_{Au}$	4.74			0.006	
	$\sigma_{C1-C36} \dots n^*_{Au}$	7.74			0.007	
	$\sigma_{C5-C36} \dots n^*_{Au}$	3.28			0.003	
	$\sigma_{C6-C36} \dots n^*_{Au}$	3.27			0.003	
	$\pi_{C6-C36} \dots n^*_{Au}$	4.86			0.006	
	$n_{Au} \dots \pi^*_{C1-C7}$	3.06			0.021	
	$n_{Au} \dots \pi^*_{C6-C36}$	3.08			0.021	
GR–Au ₂ -h	$\sigma_{C1-C2} \dots n^*_{Au}$	2.01	0.091	–0.005	0.002	–13.57
	$\sigma_{C1-C36} \dots n^*_{Au}$	2.11			0.001	
	$\sigma_{C2-C3} \dots n^*_{Au}$	2.01			0.002	
	$\sigma_{C3-C4} \dots n^*_{Au}$	2.03			0.001	
	$\sigma_{C4-C5} \dots n^*_{Au}$	2.04			0.001	
	$\sigma_{C5-C36} \dots n^*_{Au}$	1.94			0.002	
GR–Au ₂ -t	$\sigma_{C4-C5} \dots n^*_{Au}$	5.29	0.158	0.004	0.005	–23.87
	$\pi_{C5-C11} \dots n^*_{Au}$	10.83			0.013	
	$\sigma_{C5-C11} \dots n^*_{Au}$	5.02			0.005	
	$\pi_{C5-C11} \dots \sigma^*_{Au-Au}$	8.62			0.022	
	$\sigma_{C5-C36} \dots n^*_{Au}$	5.31			0.005	
	$n_{Au} \dots \sigma^*_{C5-C11}$	5.66			0.039	

^a $\Delta q_{Au_2} = q_{Au_2}(\text{complexed}) - q_{Au_2}(\text{isolated})$.

total values of Δq_{CT} with binding energies in GY–Au₂ and GR–Au₂ complexes indicates that these values increased by increasing the binding energies. The Δq_{CT} values for GY–Au₂ complexes are about 45% more than those of the GR–Au₂ complexes. Therefore, Au₂ cluster mostly behaves as a good donor in the interaction with graphyne.

(b) *Atoms in molecules analysis.* In Bader's topological QTAIM analysis [49,57], the nature of bonding interaction was analyzed in terms of the properties of electron density and its derivatives. Values for electron densities, $\rho(r)$, and their Laplacians, $\nabla^2 \rho(r)$, and

electronic energy densities, $H(r)$, for bond (BCPs) and ring critical (RCPs) points in complexes of Au₂ cluster with GY and GR are given in Table 4. Moreover, distribution of critical points in GY–Au₁₋₃ and GR–Au₂ complexes are shown in Fig. S5.

As shown in this table, values of the electron density, $\rho(r)$, for Au–C bond and ring critical points varied between 0.07 and 0.11 a.u. It is worth to mention that electron densities at these critical points are good measure of bonding strengths. Furthermore, the GY–Au₂ complexes have more values for electron densities $\rho(r)$ than GR–Au₂ complexes.

Table 4

Bond critical point data (in a.u.) from QTAIM analysis.

Complex	BCP	$\rho(r)$	$\nabla^2 \rho(r)$	$H(r)$
GY–Au ₂ -a	C ₃₃ ...Au	0.108	0.257	–0.039
	C ₃₄ ...Au	0.108	0.255	–0.039
GY–Au ₂ -b	C ₂ ...Au	0.092	0.170	–0.031
GY–Au ₂ -c	C ₃₃ ...Au	0.027	0.068	–0.001
	C ₃₂ ...Au	0.026	0.067	–0.001
	C ₃₆ ...Au	0.027	0.068	–0.001
GR–Au ₂ -b	C ₁ ...Au	0.070	0.176	–0.016
	C ₃₆ ...Au	0.071	0.174	–0.016
GR–Au ₂ -h	CCP	0.017	0.077	–0.001
GR–Au ₂ -t	C ₅ ...Au	0.084	0.161	–0.027

Table 5
Energy decomposition analysis for GY–Au₂ and GR–Au₂ complexes (in kcal/mol).

Complex	ΔE_{Pauli}	ΔE_{elstat}	ΔE_{orb}	ΔE_{disp}	ΔE_{int}	E_{b}
GY–Au ₂ –a	231.98	–162.52 (63.0%)	–93.97 (37.0%)	–13.84	–38.35	–32.68
GY–Au ₂ –b	183.55	–122.43 (62.0%)	–76.01 (38.0%)	–6.20	–21.09	–24.99
GY–Au ₂ –c	62.64	–44.77 (62.0%)	–27.52 (38.0%)	–10.14	–19.79	–20.89
GR–Au ₂ –b	111.93	–73.02 (59.0%)	–49.84 (41.0%)	–10.38	–21.31	–23.27
GR–Au ₂ –h	56.92	–34.16 (56.9%)	–25.32 (42.6%)	–16.03	–18.59	–13.57
GR–Au ₂ –t	107.22	–70.17 (60.0%)	–47.60 (40.0%)	–10.45	–21.00	–23.87

On the other hand, Laplacian of $\rho(r)$ is related to the bond interaction energy by local expression of virial theorem [60,61]. A positive value of $\nabla^2\rho(r)$ shows a depletion of electronic charge along the bond and closed-shell electrostatic interaction. In an electron-sharing (or covalent) interaction $\nabla^2\rho(r)$ has a negative value indicates that electronic charge is concentrated in the inter-nuclear region [58]. The electronic energy density, $H(r)$, at bond critical point is defined as summation of the kinetic and potential energy densities ($G(r)$ and $V(r)$, respectively) [57]. The electronic energy density can be used to compare the $G(r)$ and $V(r)$ on an equal footing. For all the interactions with significant sharing of electrons, $H(r)$ is negative, and its absolute value reflects covalent character of the interaction. A positive value of $\nabla^2\rho(r)$ at the BCPs for various Au–C bonds indicates that this interaction should be classified as a closed-shell or electrostatic interactions (see Table 4 for more

details). On the other hand, negative values of $H(r)$ for these Au–C bonds imply the covalent nature of these corresponding bonds.

3.3. Energy decomposition analysis

The nature of interactions in GY–Au₂ and GR–Au₂ complexes has been examined by means of energy decomposition analysis (EDA). In this method, the interaction energy between two fragments, ΔE_{int} , is split up into three and also four physical meaningful components:

$$\Delta E_{\text{int}} = \Delta E_{\text{Pauli}} + \Delta E_{\text{elstat}} + \Delta E_{\text{orb}} + \Delta E_{\text{disp}}$$

The first term, Pauli repulsion, comprises the destabilizing interactions between occupied orbitals and is responsible for

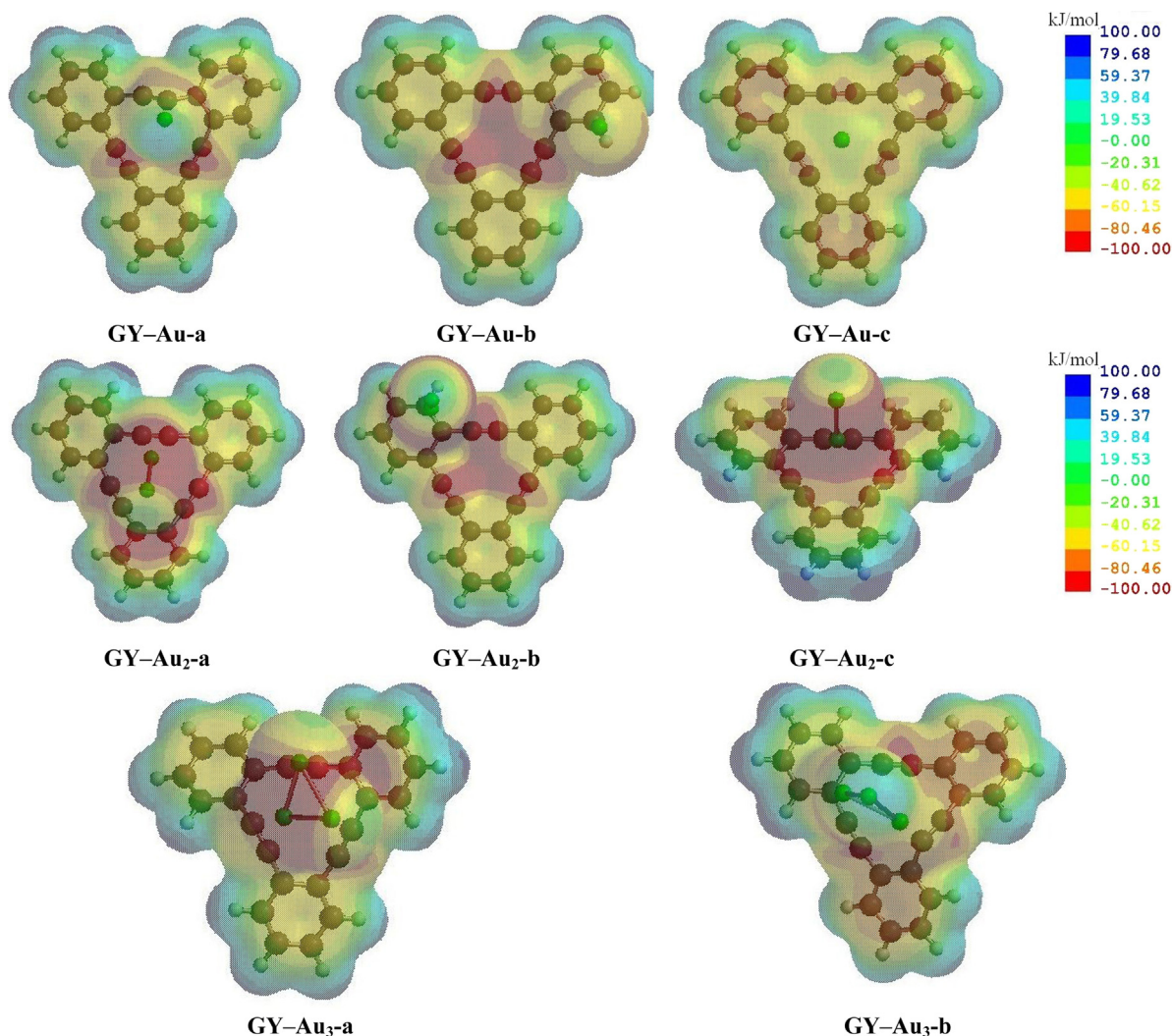


Fig. 3. Electrostatic potentials plots (ESPs) for investigated GY–Au_{1–3} complexes. ESPs are mapped on electron density isosurfaces (0.02 e/au³) for GY–Au_{1–3} complexes.

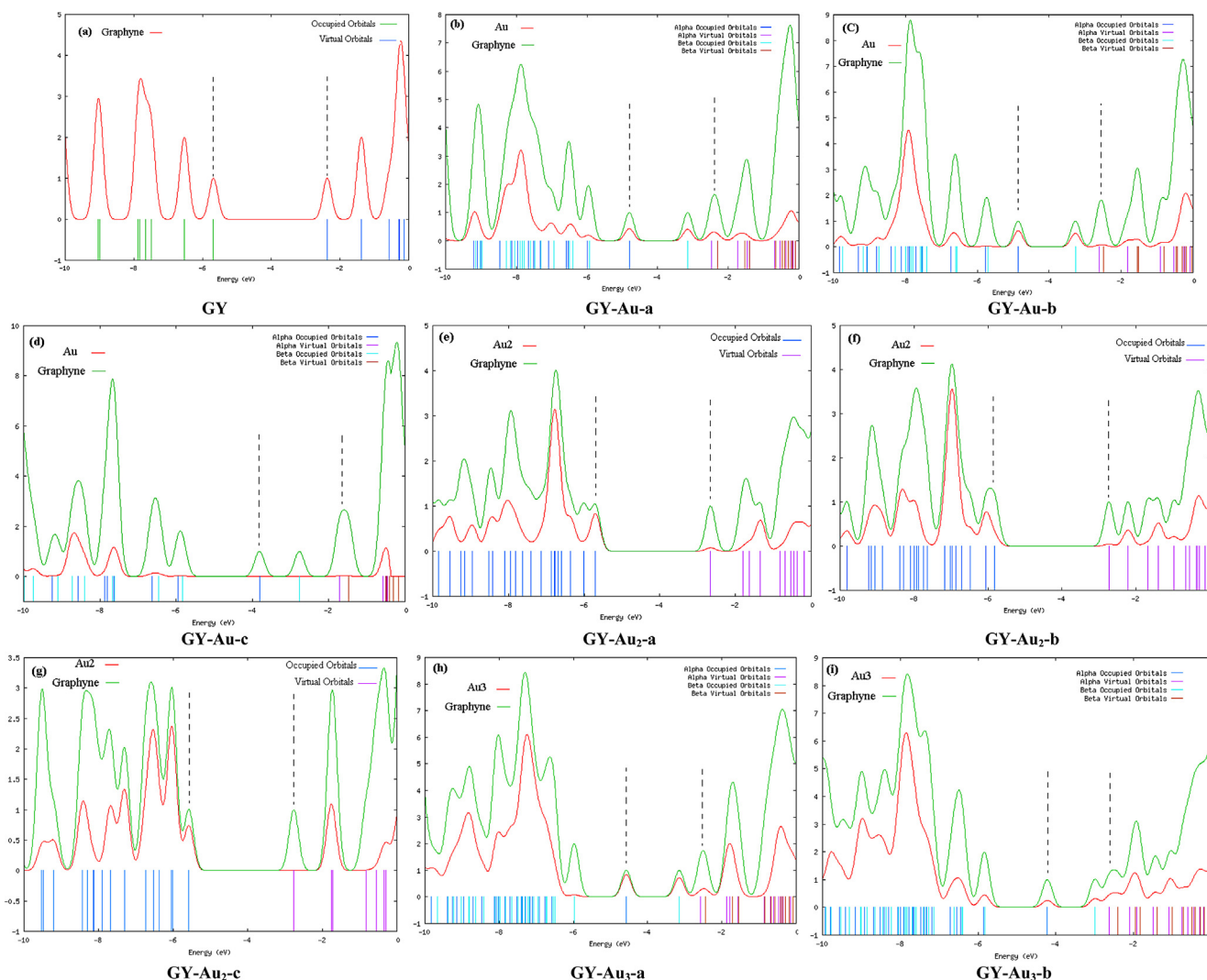


Fig. 4. Density of state (DOS) for graphyne (a) and partial density of states (PDOSs) for GY–Au_{1–3} complexes (b–i). Band gap is marked by the vertical dotted lines.

the steric repulsion. The second attractive term corresponds to the classical electrostatic interaction between the unperturbed charge distributions of the prepared (i.e. deformed) bases. The third term is the orbital interaction accounts for charge transfer (i.e., donor–acceptor interactions between occupied orbitals on one moiety with unoccupied orbitals of the other) and polarization (empty/occupied orbital mixing on one fragment due to the presence of another fragment). The last term ΔE_{disp} has been calculated when the dispersion corrected density functional has been used.

In Table 5, we summarize the contribution of these terms in the ΔE_{int} energies of GY–Au₂ and GR–Au₂ complexes obtained at the BP86–D3/TZ2P level. As you can find, these interactions arise mainly from the repulsive term, ΔE_{Pauli} , which can be explained by the number of lone pair electrons of the Au atom. Based on these results, ΔE_{elstat} and ΔE_{orb} parameters play important role in stabilization of GY–Au₂ and GR–Au₂ complexes. These interactions are more electrostatic in nature due to larger contribution of ΔE_{elstat} term than ΔE_{orb} term to the binding energy. It is worth to mention that in GR–Au₂ complexes the contribution of orbital energy (ΔE_{orb}) to the total interaction energy is more than GY–Au₂ complexes. On the other hands, stabilization of interaction due to the considering dispersion effect is not neglectable. In GY–Au₂ and GR–Au₂ complexes, interaction energies increase between –6.0 and –12.0 kcal/mol by considering dispersion. These calculations

reveal that ΔE_{elstat} , ΔE_{orb} and ΔE_{disp} account for the 58%, 35% and 7% of the attractive interactions, respectively.

To further examine the relationship between the interaction energy and its electrostatic nature in graphyne–Au_{1–3} complexes the electrostatic potential maps for these complexes were computed and shown in Fig. 3. These colorful plots have proved invaluable information in analyses of many non-covalent interactions and provide us a clear indication of how Au_{1–3} clusters could interact with graphyne surface. Comparisons of ESP for graphyne (Fig. 1) with graphyne–Au_{1–3} complexes revealed that interaction of gold clusters change the electrostatic potential of graphyne significantly. For example, as mentioned in previous part, below and above the hollow sites of $-sp$ and $-sp^2$ -bonded hexagons of graphyne, is the most electron rich region in this molecule. When Au atom placed in this region (for example in GY–Au–c complex) charge transferred from graphyne surface to gold atom. So this would change the distribution of electrostatic potential in other parts of graphyne surface. For example, comparison the ESP of graphyne with GY–Au–c complex (in Fig. 3) revealed that after complexation the most electron population increased in rich region the center of the aromatic rings of graphyne. The electrostatic potential changes in graphyne surface have the same trends as binding energies of complexes (E_b). Generally, the higher interaction energies of graphyne–Au_{1–3} complexes imply significant changes in electrostatic potential in graphyne surface.

To clarify the influence of Au_{1-3} complexation on electronic structure of graphyne the total density of states (DOS) for graphyne and the partial density of states (PDOS) for graphyne– Au_{1-3} complexes calculated and presented in Fig. 4. Therefore, we can find the contribution percentage of these fragments to each molecular orbitals of the complex (with the PDOS). It is worth to mention that the band gap is marked by the vertical dotted lines in PDOS plots. These plots were visualized with Gauss Sum software [62]. As shown in Fig. 4, the band gap of graphyne (panel (a) of Fig. 4) decreased as well as moved to positive values as result of interaction with Au atom (panels (b–d) of Fig. 4). Comparison of the band gaps of Au–graphyne complexes (GY–Au-a, GY–Au-b and GY–Au-c) with graphyne revealed that during the complexation the most significant change in the band gap observed in GY–Au-c complex. This trend confirmed with Δq cluster values given in Table 2. As shown in this table, the interacting Au atom carries a positive charge after complexation in these structures. Therefore, the band gap changes of graphyne are related to the values of transferred charge in donation and back donation processes of graphyne– Au_{1-3} complexes.

In graphyne– Au_2 complexes (GY– Au_2 -a, GY– Au_2 -b and GY– Au_2 -c complexes) the absolute values of $\Delta q_{\text{cluster}}$ ($|\Delta q_{\text{cluster}}|$) are small (0.025–0.091 e). Therefore, the band gap of graphyne was not significantly change after complexation with Au_2 cluster. It is worth to mention that in the GY– Au_2 -c complex in which charge is transferred from graphyne to gold cluster ($\Delta q_{\text{cluster}} = -0.091$ e), the band gap of graphyne was slightly moved to negative value after complexation (see panels (a) and (g) of Fig. 4 for more details). The GY– Au_3 -a and GY– Au_3 -b complexes have positive values for $\Delta q_{\text{cluster}}$ ($\Delta q_{\text{cluster}} = 0.113$ and 0.418 e, respectively). Thus, the band gap of graphyne decreased and moved to the positive value as a result of interaction with Au_3 clusters in these complexes.

4. Conclusion

In summary, we have studied interactions of small gold clusters with graphyne by using density functional theory (PBE, PBE-D3, and B3LYP-D3). Structural parameters, binding energies, and vibrational frequencies of the GY– Au_{1-3} complexes have been investigated. Results of this study indicated that gold atom and its clusters have a good tendency for interaction with graphyne and values of binding energies for GY– Au_{1-3} complexes are located in the range of -16.6 to -44.8 kcal/mol.

The nature of binding for graphyne– Au_2 and graphene– Au_2 complexes is interpreted by means of NBO, QTAIM, and EDA analyses. The NBO analysis indicates that for most of the complexes charge transferred from lone pair of Au_2 cluster to anti-bonding orbitals of the C–C bond (σ^* and π^*), and also there is back donation from σ and π binding orbitals of the C–C bond to the anti-bonding σ^* and π^* orbitals of gold cluster. Moreover, in the most of these complexes the amount of transferred charge from Au_2 to GY and GR are dominant and gold metal cluster carries a positive charge after complexation. In addition, ΔE_{CT} values have the same trend as binding energies in these complexes.

Results of QTAIM analysis revealed that Au–C bonds in investigated complexes have positive and negative values for $\nabla^2 \rho(r)$ and $H(r)$, respectively. Therefore, these bonds are partially electrostatic and partially covalent character. Our results indicated that in GY(GR)– Au_2 complexes electrostatic term has dominant contribution (58%) respect to the covalent contribution (35%). Therefore, these interactions are more electrostatic than covalent.

Acknowledgments

Support from Chemistry and Chemical Engineering Research Center of Iran is gratefully acknowledged. We appreciate the

computing resources of the Department of Chemistry University of Basel.

Appendix A. Supplementary data

Supplementary data associated with this article can be found, in the online version, at <http://dx.doi.org/10.1016/j.jmgm.2014.09.004>.

References

- [1] J. Hu, T.W. Odom, C.M. Lieber, Chemistry and physics in one dimension: synthesis and properties of nanowires and nanotubes, *Acc. Chem. Res.* 32 (1999) 435–445.
- [2] T.W. Odom, J. Huang, P. Kimm, C.M. Lieber, Structure and electronic properties of carbon nanotubes, *J. Phys. Chem. B* 104 (2000) 2794–2809.
- [3] C.H. Lui, L. Liu, K.F. Mak, G.W. Flynn, T.F. Heinz, Ultraflat graphene, *Nature* 462 (2009) 339–341.
- [4] N. Narita, S. Nagai, S. Suzuki, K. Nakao, Optimized geometries and electronic structures of graphyne and its family, *Phys. Rev. B* 58 (1998) 11009–11014.
- [5] J. Kang, J. Li, F. Wu, S.S. Li, J.B. Xia, Elastic, electronic, and optical properties of two-dimensional graphyne sheet, *J. Phys. Chem. C* 115 (2011) 20466–20470.
- [6] K. Srinivasu, S.K. Ghosh, Graphyne and graphdiyne: promising materials for nanoelectronics and energy storage applications, *J. Phys. Chem. C* 116 (2012) 5951–5956.
- [7] R.H. Baughman, H. Eckhardt, M. Kertesz, Structure–property predictions for new planar forms of carbon: layered phases containing sp^2 and sp atoms, *J. Chem. Phys.* 87 (1987) 6687–6699.
- [8] T. Yoshimura, A. Inaba, M. Sonoda, K. Tahara, Y. Tobe, R.V. Williams, Synthesis and properties of trefoil-shaped Tris(hexamethylenetriphenyl) and Tris(tetradecahydrotribenzol[12]annulene), *Org. Lett.* 8 (2006) 2933–2936.
- [9] G.X. Li, Y.L. Li, H.B. Liu, Y.B. Guo, Y.J. Li, D.B. Zhu, Graphene chemistry: theoretical perspectives, *Chem. Commun.* 46 (2012) 3256–3258.
- [10] X. Qian, Z. Ning, Y. Li, H. Liu, C. Ouyang, Q. Chen, Y. Li, Construction of graphdiyne nanowires with high-conductivity and mobility, *Dalton Trans.* 41 (2012) 730–733.
- [11] S. Wang, L.X. Yi, J.E. Halpert, X.Y. Lai, Y.Y. Liu, H.B. Cao, R.B. Yu, D. Wang, Y.L. Li, A novel and highly efficient photocatalyst based on P25–graphdiyne nanocomposite, *Small* 8 (2012) 265–271.
- [12] M.M. Haley, S.C. Brand, J.J. Pak, Carbon networks based on dehydrobenzoannulenes: preparation of substructures of graphdiyne, *Angew. Chem. Int. Ed.* (1997) 836–838.
- [13] A.K. Nair, S.W. Cranford, The minimal nanowire: mechanical properties of carbene, *EPL* 95 (2011) 16002–16006.
- [14] W.A. Chalifoux, R.R. Tykwinski, Synthesis of polyynes to model the sp-carbon allotrope carbene, *Nat. Chem.* 2 (2010) 967–971.
- [15] V.R. Coluci, S.F. Braga, S.B. Legoas, D.S. Galvao, R.H. Baughman, New families of carbon nanotubes based on graphyne motifs, *Nanotechnology* 15 (2004) 142–149.
- [16] E.H.L. Falcao, F. Wudl, Gold nanoparticle decoration of carbon nanotubes and graphyne: synthesis, physical–chemical characterization, and applications, *J. Chem. Technol. Biotechnol.* 82 (2007) 524–531.
- [17] A. Hirsch, The era of carbon allotropes, *Nat. Mater.* 9 (2010) 868–871.
- [18] A.N. Enyashin, A.L. Ivanovskii, Graphene allotropes, *Phys. Status Solidi B* 248 (2011) 1879–1883.
- [19] D. Malko, C. Neiss, F. Vines, A. Gorling, Competition for graphene: graphynes with direction-dependent dirac cones, *Phys. Rev. Lett.* 108 (2012) 086804–086809.
- [20] G.X. Li, Y.L. Li, H.B. Liu, Y.B. Guo, Y.J. Li, D.B. Zhu, Architecture of graphdiyne nanoscale films, *Chem. Commun.* 46 (2010) 3256–3258.
- [21] H. Zhang, M. Zhao, X. He, Z. Wang, X. Liu, High mobility and high storage capacity of lithium in sp-sp^2 hybridized carbon network: the case of graphyne, *J. Phys. Chem. C* 115 (2011) 8845–8850.
- [22] C. Li, J. Li, F. Wu, S.S. Li, J.B. Xia, L.W. Wang, High capacity hydrogen storage in Ca decorated graphyne: a first-principles study, *J. Phys. Chem. C* 115 (2011) 23221–23225.
- [23] Y. Jiao, A.J. Du, M. Hankel, Z.H. Zhu, V. Rudolph, S.C. Smith, Graphdiyne: a versatile nanomaterial for electronics and hydrogen purification, *Chem. Commun.* 47 (2011) 11843–11845.
- [24] L.D. Pan, L.Z. Zhang, B.Q. Song, S.X. Du, H.J. Gao, Graphyne- and graphdiyne-based nanoribbons: density functional theory calculations of electronic structures, *Appl. Phys. Lett.* 98 (2011) 173102–173103.
- [25] M.Q. Long, L. Tang, D. Wang, Y.L. Li, Z.G. Shuai, Electronic structure and carrier mobility in graphdiyne sheet and nanoribbons: theoretical predictions, *ACS Nano* 5 (2011) 2593–2600.
- [26] G.X. Li, Y.L. Li, X.M. Qian, H.B. Liu, H.W. Lin, N.Y. Chen, J. Li, Electronic structure and carrier mobility in graphdiyne sheet and nanoribbons: theoretical predictions, *J. Phys. Chem. C* 115 (2011) 2611–2615.
- [27] G.F. Luo, X.M. Qian, H.B. Liu, R. Qin, J. Zhou, L.Z. Li, Z.X. Gao, E.G. Wang, W.N. Mei, J. Lu, Y.L. Li, S. Nagase, Quasiparticle energies and excitonic effects of the two-dimensional carbon allotrope graphdiyne: theory and experiment, *Phys. Rev. B: Condens. Matter. Phys.* 84 (2011) 075439–075445.

- [28] G. Giovannetti, P.A. Khomyakov, G. Brocks, V.M. Karpan, J. van den Brink, P.J. Kelly, Doping graphene with metal contacts, *Phys. Rev. Lett.* 101 (2008) 0268031–0268038.
- [29] W. Zhu, D. Neumayer, V. Perebeinos, P. Avouris, Silicon nitride gate dielectrics and band gap engineering in graphene layers, *Nano Lett.* 10 (2010) 3572–3576.
- [30] W. Han, K. Pi, K.M. McCreary, Y. Li, J.J.I. Wong, A.G. Swartz, R.K. Kawakami, Magnetic moment formation in graphene detected by scattering of pure spin currents, *Phys. Rev. Lett.* 105 (2010) 1672021–1672026.
- [31] C.S. Shan, H.F. Yang, D.X. Han, Q.X. Zhang, A. Ivaska, L. Niu, Graphene/AuNPs/chitosan nanocomposites film for glucose biosensing, *Biosens. Bioelectron.* 25 (2010) 1070–1074.
- [32] Z.G. Xiong, L.L. Zhang, J.Z. Ma, X.S. Zhao, Photocatalytic degradation of dyes over graphene–gold nanocomposites under visible light irradiation, *Chem. Commun.* 46 (2010) 6099–6101.
- [33] H. Junjie, Sh.Y. Ma, P. Zhou, C.X. Zhang, Cha. He, L.Z. Sun, Magnetic properties of single transition-metal atom adsorbed graphdiyne and graphyne sheet from DFT+U calculations, *J. Phys. Chem. C* 116 (2012) 26313–26321.
- [34] J. Li, M.L. Hu, Z. Yu, J.X. Zhong, L.Z. Sun, Structural, electronic and magnetic properties of single transition-metal adsorbed BN sheet: a density functional study, *Chem. Phys. Lett.* 532 (2012) 40–46.
- [35] J. He, P. Zhou, N. Jiao, S.Y. Ma, K.W. Zhang, R.Z. Wang, L.Z. Sun, Magnetic exchange coupling and anisotropy of 3d transition metal nanowires on graphyne, *Sci. Rep.* 4 (2014) 4014–4023.
- [36] R.S. Sundaram, M. Steiner, H.Y. Chiu, A.A. Engelbol, R. Krupke, M. Burghard, K. Kern, P. Avouris, The graphene–gold interface and its implications for nano-electronics, *Nano Lett.* 11 (2011) 3833–3837.
- [37] S. Carara, R. Batista, H. Chacham, Graphene-protected Fe layers atop Ni(111): evidence for strong Fe–graphene interaction and structural bistability, *Phys. Rev. B* 88 (2009) 165410–165417.
- [38] K.M. McCreary, K. Pi, A.G. Swartz, W. Han, W. Bao, C.N. Lau, F. Guinea, I.M. Katsnelson, R.K. Kawakami, Effect of cluster formation on graphene mobility, *Phys. Rev. B* 81 (2010) 115453–115458.
- [39] M. Amft, B. Sanyal, O.V. Eriksson, N. Skorodumova, Small gold clusters on graphene, their mobility and clustering: a DFT study, *J. Phys: Condens. Matter* 23 (2011) 205301–205309.
- [40] S. Grimme, J. Antony, S. Ehrlich, H. Krieg, Fundamentals of time-dependent density functional theory, *J. Chem. Phys.* 132 (2010) 1541041–1541049.
- [41] (a) A.D. Becke, Density-functional exchange-energy approximation with correct asymptotic behavior, *Phys. Rev. A* 38 (1988) 3098–3100;
(b) J.P. Perdew, Density-functional approximation for the correlation energy of the inhomogeneous electron gas, *Phys. Rev. B* 33 (1986) 8822–8824.
- [42] J.P. Perdew, K. Burke, M. Ernzerhof, Generalized gradient approximation made simple, *Phys. Rev. Lett.* 77 (1996) 3865–3868.
- [43] J.M. Tao, J.P. Perdew, V.N. Staroverov, G.E. Scuseria, Fundamentals of time-dependent density functional theory, *Phys. Rev. Lett.* 91 (2003) 1464011–1464014.
- [44] (a) A.D. Becke, Density-functional thermochemistry. III. The role of exact exchange, *J. Chem. Phys.* 98 (1993) 5648–5652;
(b) C. Lee, W. Yang, R.G. Parr, Development of the Colle–Salvetti correlation-energy formula into a functional of the electron density, *Phys. Rev. B* 37 (1988) 785–789.
- [45] F. Weigend, R. Ahlrichs, Balanced basis sets of split valence, triple zeta valence and quadruple zeta valence quality for H to Rn: design and assessment of accuracy, *Phys. Chem. Chem. Phys.* 7 (2005) 3297–3305.
- [46] F. Neese, ORCA: an ab initio, density functional and semiempirical program package, Version 2.9, Bonn, Germany.
- [47] A.E. Reed, L.A. Curtiss, F. Weinhold, Intermolecular interactions from a natural bond orbital, donor–acceptor viewpoint, *Chem. Rev.* 88 (1988) 899–926.
- [48] A.E. Reed, R.B. Weinstock, F. Weinhold, Natural population analysis, *J. Chem. Phys.* 83 (1985) 735–746.
- [49] R.F.W. Bader, *Atoms in Molecules: A Quantum Theory*, 1990.
- [50] R.F.W. Bader, AIM2000 Program Package, 2002.
- [51] F.M. Bickelhaupt, E.J. Baerends, Kohn–Sham density functional theory: predicting and understanding chemistry, *Rev. Comput. Chem.* 15 (2000) 1–86.
- [52] G. te Velde, F.M. Bickelhaupt, E.J. Baerends, S.J.A. van Gisbergen, C. Fonseca Guerra, J.G. Snijders, T. Ziegler, Chemistry with ADF, *J. Comput. Chem.* 22 (2001) 931–967.
- [53] ADF, 01, Theoretical Chemistry, V. U., SCM, Amsterdam, Netherlands, 2010, <http://www.scm.com>
- [54] T. Ziegler, A. Rauk, Ab initio studies of long range interactions between ethylene molecules in the multipole expansion, *Theor. Chim. Acta* 46 (1977) 39–62.
- [55] K.J. Morokuma, Ab initio calculations of potential energy surfaces in the complex plane. II. Comparison with different methods of analytic continuation, *Chem. Phys.* 55 (1973) 129–136.
- [56] C. Chang, M. Pelissier, P.H. Durand, Regular two-component Pauli-like effective Hamiltonians in Dirac theory, *Phys. Scr.* 34 (1986) 394–404.
- [57] J.L. Heully, I. Lindgren, E. Lindroth, S. Lundquist, A.J.G. Snijders, New advances in relativistic quantum chemistry, *J. Chem. Phys.* 99 (1993) 4597–4610.
- [58] E. van Lenthe, E.J. Baerends, J. Snijders, Relativistic effects in physics and chemistry of element, *J. Chem. Phys.* 105 (1996) 6505–6514.
- [59] Spartan '06V102', Wavefunction, Inc. Irvine, CA.
- [60] R.W.F. Bader, A quantum theory of molecular structure and its applications, *Chem. Rev.* 91 (1991) 893–928.
- [61] P.L.A. Popelier, *Atoms in Molecules. An Introduction*, Pearson Education, London, GB, 2000.
- [62] N. O'Boyle, GaussSum, Revision 2.1, <http://GaussSum.sf.net>